THERMOELECTRICS

Heavily doped, highly compensated epitaxial ScN thin films exceed Boltzmann thermopower limits

Renuka Karanje[1,2]†, Dheemahi Rao[1,2]†, Diksha Dadhich[1,2], Sourav Rudra[1,2], Ashalatha Indiradevi Kamalasanan Pillai[3], Magnus Garbrecht[3], Subroto Mukerjee[4], Bivas Saha[1,2,5]*

The Seebeck effect converts a temperature gradient into an electric voltage. However, conventional transport theories constrain this thermopower to a few millivolts per Kelvin in crystalline materials. We present experimental evidence of a Seebeck coefficient exceeding −124 millivolts per Kelvin near room temperature in heavily doped, highly compensated (HDHC) epitaxial scandium nitride (ScN) thin films. Random distribution of charged dopants in HDHC ScN are known to generate potential fluctuations that distort the electronic bands and give rise to percolative transport, and our results further reveal a power-law scaling between thermopower and electrical conductivity. In ultrathin films, the Rytova-Keldysh modifications of the Coulomb potential further amplify the potential fluctuations and enhance the Seebeck response. Our findings reveal a solid-state analog of electrolyte-like thermopower in a crystalline semiconductor.

The Seebeck effect, in which a temperature difference (ΔT) across the junction of two dissimilar materials generates a voltage difference (ΔV), enables the direct conversion of heat into electricity (Fig. 1A) (*1*, *2*). This voltage arises from the movement of charge carriers between regions of differing temperatures. The resulting thermoelectric response is quantified by the Seebeck coefficient ($S = -\Delta V/\Delta T$ in the linear-response regime), which is commonly described within the Boltzmann transport framework in which each charge carrier encounters an essentially uniform environment (*3*).

Most high-conductivity metals exhibit a small S of less than a few tens of microvolts per Kelvin near room temperature. For semiconductors, S depends on the energy difference between the conduction or valence band edge (E_{edge}) and the Fermi level (E_F) and increases as the E_F moves closer to the middle of the bandgap (*4*, *5*). Further, Boltzmann transport theory predicts an upper bound for S of a few millivolts per Kelvin near room temperature, which restricts S in most semiconductors (*5*). Overcoming such limitations on S will lead to new generations of temperature sensors (*6*), cryogenic thermoelectric single-photon detectors (*7*), and high-efficiency thermoelectric materials with applications ranging from quantum sensing to energy harvesting (*8*).

Large S values beyond conventional band transport limits have been reported for high-purity, low–carrier-density C_{60} and small organic molecules such as pentacene, rubrene, and sumanene near room temperature (*5*, *9*). Although the underlying microscopic mechanisms for such large S values in these molecules remain unclear, the formation of small polarons and potential fluctuations at the band edges has been proposed (*5*). Exceptionally high S values exceeding several millivolts per Kelvin have been reported in intermetallic compounds and nanostructures, such as the quasi–one-dimensional conductor tetramethyltetraselenafulvalene hexafluorophosphate [$(TMTSF)_2PF_6$], $FeSb_2$, copper sulfides and selenides, and silicene-based systems, albeit at low temperatures (10 to 100 K) (*10*–*13*). Diverse mechanisms, including phonon drag (*11*, *14*), resonant scattering (*15*), Kondo effects (*16*), phase transitions (*17*), sharp features in the electronic density of states (*18*), and spin fluctuations (*10*), have been proposed as the origin of the large S values in these materials.

Although electron or hole transport in most inorganic solid-state materials typically results in S values between 100 and 500 $\mu V\ K^{-1}$ near room temperature, ionic conductors in electrolytes, such as poly(styrene sulfonic acid) (PSSH) hydrogels, poly(ethylene oxide)-sodium hydroxide (PEO-NaOH), and ionic gelatin, exhibit S in the millivolts per Kelvin range due to the Soret effect (thermally driven ion diffusion), thermogalvanic effects, or mixed ionic-electronic conduction (*19*, *20*). Identifying inorganic single-crystalline semiconductors with exceptionally large S could enable practical applications such as ultrasensitive temperature sensing, low-noise thermal imaging, high-resolution heat flux detection, suspended bolometric device, and Internet-of-Things sensors (*19*, *21*).

Heavily doped, highly compensated (HDHC) semiconductors are materials in which a spatially inhomogeneous distribution of charged dopants leads to large-scale potential fluctuations, an effect that could achieve large S values (*5*, *22*). Random potential fluctuations break translational symmetry and rupture the valence and conduction band edges in HDHC semiconductors, which leads to the breakdown of the Fermi sea and causes carrier localization in isolated metallic puddles surrounded by potential barriers (Fig. 1, B to D, and section II-A in the supplementary materials) (*22*, *23*). Because carriers must hop at lower temperatures or percolate at sufficiently higher activation energies from droplet to droplet, HDHC semiconductors exhibit a metallic-to-activated quasiclassical Anderson transition (QAT) (*22*, *24*, *25*). Such disorder and random potential fluctuations cause electron transport in HDHC semiconductors to deviate from the conventional one-electron band structure and the limits set by the Boltzmann transport theory (*3*, *22*).

Scandium nitride (ScN), a refractory group-III(B) transition metal pnictide, can be used to study charged dopant-induced potential fluctuations and their impact on transport properties (*24*). Unintentional incorporation of oxygen impurities cause as-deposited ScN epitaxial thin films to become HD n-type semiconductors (*26*–*28*). However, Mg-hole doping can reduce its high carrier concentration and lead to a distinct metallic-to-activated transport transition accompanied by a nine orders of magnitude increase in resistivity at room temperature, exhibiting the QAT in HDHC ScN films (*24*). Consistent with the theoretical predictions, HDHC ScN exhibits a transition from the low-temperature hopping conduction to a thermally activated percolative transport with increasing temperature, anomalously low electronic mobility that increases with rising temperature, persistent photoconductivity lasting for several days (*29*), and a sign reversal of the thermopower in a moderately compensated ScN film with an S of –5.7 $mV\ K^{-1}$ near room temperature (*24*).

We now show that an S value exceeding –124 $mV\ K^{-1}$ can be achieved in ~200-nm-thick HDHC ScN thin films at ambient temperature. Further, our results show that in ultrathin HDHC films, dimensionality reduction induces Rytova-Keldysh modification of Coulomb interactions, amplifying the potential fluctuations and driving a nondegenerate semiconducting to QAT electronic transition with substantially enhanced thermopower at comparable compensation levels.

Colossal thermopower in HDHC ScN films

Mg-hole–doped, ~200-nm-thick ScN films were deposited on (001) MgO substrates with ultrahigh vacuum magnetron sputtering at a base pressure of 1×10^{-9} Torr and 850°C substrate temperature [see (*24*) and section I-A in the supplementary materials for the deposition method). Spectroscopic and microscopic characterizations revealed that Mg-hole dopants were uniformly distributed inside ScN without any precipitation or secondary phase formation, as discussed below. Because of the low

[1]Chemistry and Physics of Materials Unit, Jawaharlal Nehru Centre for Advanced Scientific Research, Bangalore, India. [2]International Centre for Materials Science, Jawaharlal Nehru Centre for Advanced Scientific Research, Bangalore, India. [3]Sydney Microscopy and Microanalysis, The University of Sydney, Camperdown, NSW, Australia. [4]Department of Physics, Indian Institute of Science, Bangalore, India. [5]School of Advanced Materials (SAMat), Jawaharlal Nehru Centre for Advanced Scientific Research, Bangalore, India. *Corresponding author. Email: bsaha@jncasr.ac.in or bivas.mat@gmail.com †These authors contributed equally to this work.

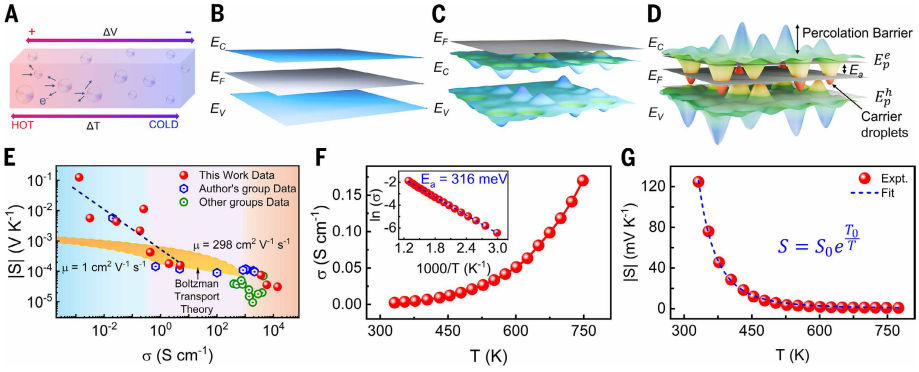

Fig. 1. Colossal Seebeck effect in HDHC ScN thin films. (**A**) Schematic of the Seebeck effect, in which a temperature difference (ΔT) across the junction between two conductors leads to a voltage difference (ΔV). In HDHC semiconductors, real-space potential fluctuations lead to metallic droplets (bubbles) surrounded by potential barriers. (**B**) In intrinsic semiconductors, the energy bands are flat in real space, with E_F lying midway between the conduction band (E_C) and valence band (E_V). (**C**) In HD *n*-type semiconductors, such as as-deposited ScN films, charged dopants (O_N) lead to potential fluctuations rupturing the band structure. However, such potential fluctuations are fully screened as the E_F lies inside the conduction band (CB). (**D**) As E_F is lowered inside the bandgap through carrier compensation (Mg doping in HD ScN), the carriers are trapped inside the potential wells, leading to a degenerate semiconducting to QAT electronic transition and resulting in a colossal *S* near room temperature. The schematic illustrates the band diagram for the fully compensated case. (**E**) Absolute *S* near room temperature as a function of σ of various ScN films with thicknesses of ~200 nm across the degenerate semiconducting, nondegenerate Boltzmann transport regime to the QAT regime. The yellow-shaded region indicates the limits on *S* predicted from Boltzmann transport theory. For the least-conductive film (sample R1), *S* reached a colossal –124.6 mV K^{-1}. The data shown as open circles were collected from Rao *et al*. (*34*), Saha *et al*. (*27*), Burmistrova *et al*. (*35*,*37*), and Tureson *et al*. (*36*) for comparison. (**F**) Temperature-dependent σ of the least-conductive HDHC ScN film showing thermally activated percolative transport of carriers. The inset shows the percolation activation energy of 316 meV. (**G**) Temperature-dependent *S* of the same film showing a steep decrease with increasing temperature.

substitutional Mg dopant on an Sc site (Mg_{Sc}) and substitutional O dopant on an N site (O_N's) defect activation energies, most dopants were ionized at room temperature (*27*). Details of the samples, designated as R0 for HD ScN, R1 to R5 for progressively decreasing *S*, and R6 to R11 for ultrathin HDHC films, as well as the corresponding measurement methods, are provided in table S1 and sections I-B to I-E in the supplementary materials.

Plots of *S* as a function of electrical conductivity (σ) near room temperature (~350 K) revealed three distinct transport regimes in ScN films (Fig. 1E). In highly conductive HD *n*-type ScN (σ = ~10^2 to 10^4 S cm^{-1}), typically achieved in physical vapor depositions such as magnetron sputtering or molecular beam epitaxy, as well as chemical vapor deposition such as hybrid vapor phase epitaxy techniques, *S* remained moderate: in the –10 to –100 μV K^{-1} range near room temperature (*30*–*32*). Within this transport regime, *S* is mainly determined by the free electron concentration of ScN, typically in the 10^{20} to 10^{21} cm^{-3} range, and is well explained with the Boltzmann transport theory calculations (*33*). The *S* measured for the ScN films deposited in this work, data of *S* from our previous research (*24*, *27*, *34*), as well as *S* of ScN films deposited with molecular beam epitaxy, hybrid vapor phase epitaxy, and magnetron sputtering from other groups (*35*–*37*), are also presented in Fig. 1E.

As Mg-hole dopants were introduced to reduce σ (~1 to 10^2 S cm^{-1} range), *S* rose to several hundreds of microvolts per Kelvin near room temperature but remained within the limits set by the Boltzmann transport theory in the nondegenerate regime (Eq. 1), as shown by the shaded region with upper and lower bounds in Fig. 1E determined with experimental mobility for ScN (*9*, *38*). Within the relaxation time approximation of the linearized Boltzmann transport formalism, *S* is given by the following expression:

$$S = -\frac{k_B}{e}\left[\frac{5}{2} + r - \ln\frac{nh^3}{2\left(2\pi m^* k_B T\right)^{3/2}}\right] \quad (1)$$

where m^*, e, r, n, h, and k_B are the effective mass, elementary charge of an electron, exponent in the energy dependence of the relaxation time ($\tau \propto E^r$), carrier concentration, Planck's constant, and the Boltzmann constant, respectively. For acoustic deformation potential scattering, r is taken to be –0.5, consistent with the standard energy dependence of the relaxation time in three-dimensional systems with parabolic bands. Hole doping reduces carrier concentration in ScN and pushes the E_F inside the bandgap, leading to a conventional response similar to that of a nondegenerate semiconductor (*27*).

For increasing hole-dopant concentrations, as potential fluctuations dominated and ScN underwent the QAT, σ was reduced by several orders of magnitude (σ < 1 S cm^{-1}), and *S* increased by more than two orders, exceeding the traditional Boltzmann transport theory predictions (*30*). For the lowest-conductivity HDHC film with σ = 2.35 × 10^{-3} S cm^{-1}, *S* reached a value of –124.6 mV K^{-1} near room temperature. Across the three-transport regime, σ for ScN decreased by more than seven orders of magnitude and *S* increased by more than four orders. Unlike the $S \propto -\ln(\sigma)$ relations expected from the Boltzmann transport theory in the nondegenerate semiconducting regime (*3*, *9*), *S* exhibited an empirical $S \propto \sigma^{-0.66}$ power law distribution with a much stronger dependence on σ (see section II-B and fig. S2 in the supplementary materials for further discussion).

Temperature-dependent measurements further revealed that above room temperature, σ underwent a percolation activation, with $\sigma = \sigma_0 e^{-\frac{E_a}{k_B T}}$ fitting yielding an activation energy E_a of ~316 meV for the HDHC film with the lowest σ and maximum potential fluctuations (Fig. 1F). Concomitantly, *S* decreased steeply as the temperature rose (Fig. 1G). Starting from –124.6 mV K^{-1} at 350 K, *S* decreased to –11.83 mV K^{-1} at 450 K and showed relatively less change at higher temperatures. In general, *S* increases linearly with increasing temperature for high-conductivity metals or degenerate semiconductors, whereas *S* decreases as temperature increases for semiconductors in the nondegenerate regime. In materials in which strong electron correlation effects are prominent and Mott-variable range hopping or Efros-Shklovskii hopping conduction explains the transport, *S* is expected to decrease with temperature as T^α, with an α < 1 determined by the dimensionality of the system (*22*). However, the observed power law dependence of *S* on σ and percolation activation of σ yielded $S = S_0 e^{\frac{T_0}{T}}$ in HDHC ScN, which fits very well with the experiment. The sharp change in *S* with *T* suggests that temperature-controlled Seebeck switches could be developed for device applications. Temperature-dependent measurements of *S* and σ provide compelling evidence that potential fluctuations and associated percolative transport are the underlying mechanisms behind the colossal *S* observed in the HDHC ScN. Notably, despite its much lower electrical conductivity, HDHC ScN exhibits near room-temperature power factors comparable to those of HD ScN and other well-established thermoelectric materials (see section II-C and fig. S3 in the supplementary materials for details) (*8*, *34*, *39*).

Unlike HDHC ScN thin films, which exhibit a negative thermopower across the entire measured temperature range, heavily doped, moderately compensated (HDMC) ScN thin films undergo a negative-to-positive sign reversal near 600 K and exhibit a large thermopower [see fig. S4A in the supplementary materials and (*24*)]. The observed thermopower behavior, including the sign reversal, the weak temperature dependence

at elevated temperatures, and its evolution from large to colossal magnitudes, can all be qualitatively explained with the framework of the narrow-band Hubbard model originally formulated by Beni and Chaikin (*40*, *41*) (see sections II-D and II-E in the supplementary materials for details). Within this framework, the electronic system in these compensated films can be described by a single-band Hubbard Hamiltonian in which the on-site Coulomb repulsion (U) exceeds the intersite hopping between charge puddles. Using the Kubo formalism, Beni and Chaikin (*40*, *41*) derived an expression for S and predicted a universal sign change as the carrier filling increased and temperature approached the energy scale set by U. Although the magnitude of the experimentally observed S exceeded this prediction, the temperature and carrier filling–dependent crossover where S changed sign was qualitatively consistent with this model. Taken together, these observations suggest that the narrow-band Hubbard model captures the essential qualitative features of the thermoelectric response in both HDMC and HDHC films.

Colossal thermopower with sign reversal in ultrathin HDHC ScN films

The effect of film thickness and dimensionality reduction on the colossal S in HDHC ScN films was determined by depositing ultrathin films of decreasing thickness while retaining the same Mg-dopant concentrations in ScN. The Mg-hole dopant concentration was chosen such that in the thick film limit, it led to a relatively high conductivity value close to $\sim 4.6 \times 10^{-1}$ S cm^{-1} near room temperature, which falls at the boundary between the nondegenerate Mott and QAT regime (see Fig. 1E and section I-A in the supplementary materials for details). The amplitude of potential fluctuations (γ) in the presence of a low dielectric environment scales as $\gamma \propto 1/t$, where t is the film thickness. Therefore, small concentrations of impurities can cause large-scale potential fluctuation and affect S and σ in ultrathin films through the Rytova-Keldysh modification of the Coulomb potential (*42*, *43*). Thickness-dependent σ at room temperature revealed that compared with a thicker ScN, σ in ultrathin films decreased by more than four orders of magnitude (Fig. 2A). This decrease in σ was likely caused by a nondegenerate semiconducting to QAT electronic transition triggered by the dimensionality reduction–induced enhancement of potential fluctuations.

Although surface scattering of electrons also contributes to decreasing σ in ultrathin films, previous research has shown that on degenerate ScN without any Mg doping, thickness reduction from 240 to 5 nm decreases σ by ~10 times, which is much less than the decrease that we observed (*44*). The temperature dependence of σ further showed that σ in thick films (~50 nm) remained nearly invariant across the measured temperature range (50 to 400 K), whereas ultrathin films (12, 10, 7.5, 6, and 5 nm) exhibited a positive temperature coefficient of σ, underlining the onset of their insulating nature (Fig. 2B). Moreover, the thinnest 6- and 5-nm HDHC ScN films exhibited a three orders of magnitude decrease in σ as the temperature decreased from 400 to ~220 K (Fig. 2B). At lower temperatures, the measurement became limited by instrument resolution.

S in ultrathin HDHC films near room temperature far exceeded the S measured for thick ScN with similar hole doping due to their enhanced potential fluctuations. Figure 2C shows that a 7.5-nm film exhibited a colossal S of −83.41 mV K^{-1} near room temperature, which was about two orders of magnitude higher than the S obtained in thick films (Fig. 1E) but with similar compensation levels. However, temperature-dependent measurements showed that, like thick films, S of ultrathin

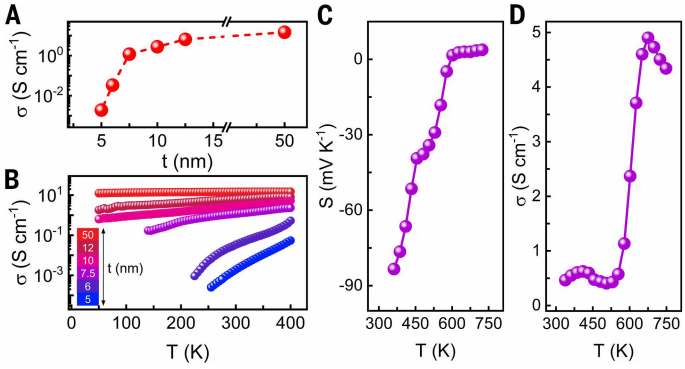

Fig. 2. Thermopower in HDHC ultrathin ScN. (**A**) σ of Mg-hole–doped ScN films decreased by four orders of magnitude as a function of the film thickness in the ultrathin regime. (**B**) Temperature-dependent σ in ultrathin ScN films showed a degenerate semiconducting type to QAT. (**C**) Temperature-dependent S of a 7.5-nm (sample R9) HDHC ScN film exhibiting colossal S near room temperature, like the HDHC 200-nm-thick film. (**D**) Temperature-dependent σ of a 7.5-nm (sample R9) HDHC ScN film exhibiting activated transport.

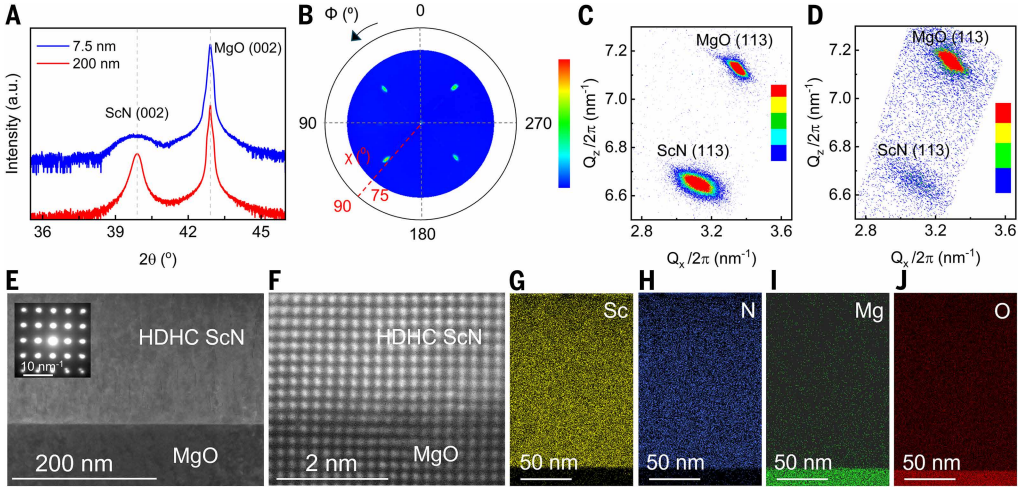

Fig. 3. Structural characterization of HDHC ScN films. (**A**) Symmetric 2θ – ω HRXRD diffractogram of a 200-nm-thick (sample R1) and a 7.5-nm ultrathin (sample R9) HDHC ScN thin film showing (002)-oriented film growth on (001) MgO substrates. (**B**) Pole-figure measurements revealed four equally spaced φ peaks that highlight the epitaxial nature of the films. (**C** and **D**) Reciprocal space x-ray mapping of 200-nm-thick (C) and 7.5-nm ultrathin (D) ScN showing that the (113) MgO and (113) ScN diffraction spots are separated along the Q_x line, which highlights their strain-relaxed nature. (**E**) HAADF-STEM micrograph of an HDHC ScN thin film showing homogeneous and uniform epitaxial growth of the film. (**F**) Atomic-resolution STEM image of the ScN/MgO interface showing cubic epitaxial growth. (**G** to **J**) STEM-EDS mapping showing a uniform distribution of Sc (G), N (H), Mg (I), and O (J) atoms inside the film.

HDHC film decreased sharply with an increase in temperature (Fig. 2C). *S* in the 7.5-nm ultrathin ScN exhibited a negative-to-positive sign reversal at ~600 K, followed by the conductivity activation evident from the temperature-dependent σ measurement (Fig. 2D).

Variations in thermopower and electrical conductivity among similar HDHC, HDMC, and HD ScN films, together with heating-cooling and temperature ramp-rate measurements, confirm the robustness of the colossal *S* in HDHC ScN and the sign reversal of thermopower in HDMC ScN (see sections II-F and II-G in the supplementary materials). Further, the technological potential of this colossal Seebeck response is illustrated through a prototype photon sensor, described in sections I-F and II-H of the supplementary materials.

Structure and microstructural characterization

We characterized the crystal structure of thick and ultrathin HDHC ScN using high-resolution x-ray diffraction (XRD) and high-resolution transmission electron microscopy (HRTEM). The symmetric 2θ – ω XRD pattern of a representative 200-nm-thick and 7.5-nm ultrathin HDHC ScN showed that the films grew perfectly with (002) orientations on (001) MgO substrates with a lattice parameter of 4.52 Å, consistent with previous reports (Fig. 3A) (*45*). Pole figure measurement revealed four equally spaced φ peaks corresponding to the (111) planes in ScN that verified their cubic symmetry and epitaxial nature (Fig. 3B).

Reciprocal space mapping (Fig. 3, C and D) further highlighted that the films were strain relaxed on the (001) MgO substrate. Notably, XRD analysis of the films, even after performing temperature-dependent *S* and σ measurements, did not show any appreciable changes, highlighting the structural robustness of the HDHC films (see section II-I in the supplementary materials). Previous synchrotron-radiation extended x-ray near-edge fine structure (EXAFS) analysis of HDHC films also revealed no appreciable changes in the bonding environment or structural distortions in ScN due to Mg-hole doping (*24*).

High-angle annular dark field-scanning transmission electron microscopy (HAADF-STEM) imaging further revealed homogeneous and uniform HDHC ScN film growth on a (001) MgO substrate (Fig. 3, E and F). The cubic electron diffraction pattern in the inset confirmed [001] (001) ScN || [001] (001) MgO epitaxy. Energy-dispersive x-ray spectroscopy (STEM-EDS) elemental mapping showed that all atoms were homogeneously distributed inside the film (Fig. 3, G to J). Therefore, HDHC ScN exhibits excellent structural qualities and is epitaxial and nominally single crystalline in nature. The HAADF-STEM imaging of ultrathin HDHC ScN also exhibited high crystalline quality and was epitaxial in nature, as presented in fig. S21. Further details on dopant concentration, distribution, interface quality, etc., are presented in sections II-I, II-J, II-K, and II-L of the supplementary materials.

Summary

We report *S* values exceeding –124 mV K^{-1} near room temperature in HDHC epitaxial ScN ultrathin films. This thermopower exceeds by nearly two orders of magnitude the values long considered attainable in solids and rivals those found in electrolytes and ionic conductors. In ultrathin films, the enhancement of potential fluctuations due to the Rytova-Keldysh potential further amplifies the Seebeck response. Our findings establish one of the highest *S* values recorded in inorganic crystalline material and unveil charged-dopant–induced potential fluctuations as a strategy for boosting thermoelectric performance.

REFERENCES AND NOTES

1. T. J. Seebeck, *Über Den Magnetismus Der Galvanischen Kette* (1822).
2. J. R. Sootsman, D. Y. Chung, M. G. Kanatzidis, *Angew. Chem. Int. Ed.* **48**, 8616–8639 (2009).
3. S. Dongmin Kang, G. Jeffrey Snyder, *Nat. Mater.* **16**, 252–257 (2017).
4. P. J. P. R. Kubo, T. Nagamiya, P. J. Price, *Phys. Today* **24**, 59–60 (1971).
5. M. Nakamura *et al.*, *Faraday Discuss.* **250**, 361–376 (2024).
6. H. Yu *et al.*, *Nat. Commun.* **15**, 2521 (2024).
7. A. Gulian, K. Wood, D. van Vechten, G. Fritz, *J. Mod. Opt.* **51**, 1467–1490 (2004).
8. Q. Yan, M. G. Kanatzidis, *Nat. Mater.* **21**, 503–513 (2022).
9. H. Kojima *et al.*, *Appl. Phys. Express* **8**, 121301 (2015).
10. Y. Machida, X. Lin, W. Kang, K. Izawa, K. Behnia, *Phys. Rev. Lett.* **116**, 087003 (2016).
11. H. Takahashi *et al.*, *Nat. Commun.* **7**, 12732 (2016).
12. D. Byeon *et al.*, *Nat. Commun.* **10**, 72 (2019).
13. T. Terada *et al.*, *Adv. Mater. Interfaces* **9**, 2101752 (2022).
14. P. Jha *et al.*, *J. Appl. Phys.* **113**, 193702 (2013).
15. A. Nadtochiy *et al.*, *Sci. Rep.* **9**, 16335 (2019).
16. J. Wu *et al.*, *Proc. Natl. Acad. Sci. U.S.A.* **117**, 13929–13936 (2020).
17. A. Jaoui *et al.*, *NPJ Quantum Mater.* **5**, 94 (2020).
18. P. Hu *et al.*, *ACS Appl. Mater. Interfaces* **11**, 34046–34052 (2019).
19. C.-G. Han *et al.*, *Science* **368**, 1091–1098 (2020).
20. B. Chen *et al.*, *Sci. Adv.* **7**, eabi7233 (2021).
21. A. Kumar, D. Sivaprahasam, A. D. Thakur, *J. Alloys Compd.* **853**, 157001 (2021).
22. B. I. Shklovskii, A. L. Efros, *Electronic Properties of Doped Semiconductors* (Springer, 1984); vol. 45 of *Springer Series in Solid-State Sciences*; http://link.springer.com/10.1007/978-3-662-02403-4.
23. V. F. Mitin, *Appl. Phys. Lett.* **92**, 2006–2009 (2008).
24. D. Rao *et al.*, *Phys. Rev. B* **109**, 155307 (2024).
25. E. Abrahams, *50 Years of Anderson Localization* (World Scientific, 2010); https://www.worldscientific.com/worldscibooks/10.1142/7663.
26. A. le Febvrier, N. Tureson, N. Stilkerich, G. Greczynski, P. Eklund, *J. Phys. D Appl. Phys.* **52**, 035302 (2019).
27. B. Saha *et al.*, *Appl. Phys. Lett.* **110**, 1–6 (2017).
28. M. A. Moram, Z. H. Barber, C. J. Humphreys, *Thin Solid Films* **516**, 8569–8572 (2008).
29. D. Rao, A. I. K. Pillai, M. Garbrecht, B. Saha, *Adv. Electron. Mater.* **9**, 2200975 (2023).
30. S. Kerdsongpanya *et al.*, *Appl. Phys. Lett.* **99**, 232113 (2011).
31. Y. Oshima, E. G. Víllora, K. Shimamura, *J. Appl. Phys.* **115**, 153508 (2014).
32. H. Al-Atabi *et al.*, *Appl. Phys. Lett.* **116**, 132103 (2020).
33. B. Saha *et al.*, *Phys. Rev. B* **97**, 085301 (2018).
34. D. Rao *et al.*, *Appl. Phys. Lett.* **116**, 152103 (2020).
35. P. V. Burmistrova *et al.*, *J. Appl. Phys.* **113**, 153704 (2013).
36. N. Tureson *et al.*, *Phys. Rev. B* **98**, 205307 (2018).
37. P. V. Burmistrova *et al.*, *J. Mater. Res.* **30**, 626–634 (2015).
38. G. B. Rayner Jr. *et al.*, *J. Vac. Sci. Technol. A* **43**, 020401 (2025).
39. G. Tan, L. D. Zhao, M. G. Kanatzidis, *Chem. Rev.* **116**, 12123–12149 (2016).
40. G. Beni, *Phys. Rev., B, Solid State* **10**, 2186–2189 (1974).
41. P. M. Chaikin, G. Beni, *Phys. Rev., B, Solid State* **13**, 647–651 (1976).
42. Y. Huang, Y. Ayino, B. I. Shklovskii, *Phys. Rev. Mater.* **5**, 044606 (2021).
43. L. V. Keldysh, *JETP Lett.* **29**, 658–661 (1979).
44. D. Mukhopadhyay, S. Rudra, B. Biswas, P. Das, B. Saha, *Appl. Phys. Lett.* **123**, 192101 (2023).
45. A. R. Smith, H. A. H. AL-Brithen, D. C. Ingram, D. Gall, *J. Appl. Phys.* **90**, 1809–1816 (2001).
46. R. Karanje, Data for: Heavily doped, highly compensated epitaxial ScN thin films exceed Boltzmann thermopower limits, Zenodo (2026); https://doi.org/10.5281/zenodo.19594206.

ACKNOWLEDGMENTS

Funding: R.K., D.R., and B.S. are supported by the International Centre for Materials Science (ICMS) and Sheikh Saqr Laboratory (SSL) of Jawaharlal Nehru Centre for Advanced Scientific Research (JNCASR). B.S. is supported by the Ras Al Khaimah Centre for Advanced Materials, Stevin Rock, LLC, and Raknor, LLC, and the Anusandhan National Research Foundation (ANRF) of the Department of Science and Technology (DST) in India (Core Research Grant CRG/2023/007061). R.K., D.R., D.D., and B.S. acknowledge the SAMat Research Facilities, JNCASR, Bengaluru, for providing access to the experimental characterization facilities used in this work. R.K., D.R., and D.D. are supported by a fellowship from JNCASR. S.R. is supported by a fellowship from the Council of Scientific & Industrial Research (CSIR). M.G. and A.I.K.P. acknowledge Sydney Microscopy and Microanalysis at the University of Sydney for access to electron microscopy facilities and technical support. **Author contributions:** D.R. and B.S. conceived the project. R.K. and D.R. deposited thin films and performed thermopower measurements and electrical characterizations. R.K. performed structural characterization. D.D. fabricated and measured the Seebeck sensor devices. S.R. conceptualized the empirical model for describing the experimental results. A.I.K.P. performed the TEM sample preparation. M.G. performed TEM imaging and analysis. S.M. provided valuable insight into interpretation of the experimental results. All authors discussed and contributed to the preparation of the manuscript. **Competing interests:** B.S., R.K., and D.R. filed an Indian Patent Application (20264104017) (pending) on thermoelectric thin film materials and sensors for temperature and photon detection. The remaining authors declare no competing interests. **Data, code, and materials availability:** All data and descriptions of new materials required to evaluate the conclusions in this study are available in the main text or the supplementary materials and in the dataset available at Zenodo (*46*).

SUPPLEMENTARY MATERIALS

science.org/doi/10.1126/science.aef9458
Materials and Methods; Supplementary Text; Figs. S1 to S23; Tables S1 to S3; References; Movies S1 and S2

Submitted 29 January 2026; accepted 16 June 2026

10.1126/science.aef9458

Heavily doped, highly compensated epitaxial ScN thin films exceed Boltzmann thermopower limits

Renuka Karanje, Dheemahi Rao, Diksha Dadhich, Sourav Rudra, Ashalatha Indiradevi Kamalasanan Pillai, Magnus Garbrecht, Subroto Mukerjee, and Bivas Saha

Science **393** (6811), . DOI: 10.1126/science.aef9458

Editor's summary

Although Seebeck coefficients in the millivolts per Kelvin range are observed for ionic conductors, electronic conductors are usually limited by Boltzmann transport theory to the microvolts per Kelvin range. Karanje *et al*. grew 200-nanometer-thick scandium nitride films that had a spatially inhomogeneous distribution of charged dopants. These films could undergo large-scale potential fluctuations that overcome the Boltzmann limit. A Seebeck coefficient exceeding #124 millivolts per Kelvin was seen near room temperature. —Phil Szuromi

Science (ISSN 1095-9203) is published by the American Association for the Advancement of Science. 1200 New York Avenue NW, Washington, DC 20005. The title *Science* is a registered trademark of AAAS.